

Analysis of light-emission enhancement of low-efficiency quantum dots by plasmonic nano-particle

Jinxi Huang,^{1,2} Hao Hu,^{1,2} Zhewei Wang,¹ Wenyuan Li,¹ Ji Cang,¹ Jianqi Shen,¹ and Hui Ye^{1,*}

¹*State Key Laboratory of Modern Optical Instrumentation, College of Optical Science and Engineering, Zhejiang University, Hangzhou, 310027, China*

²*J. H. and H. H. contributed equally*

[*huiye@zju.edu.cn](mailto:huiye@zju.edu.cn)

Abstract: In this paper, a nano-pillar array integrated near quantum dots (QDs), which serves as a Purcell cavity as well as a column antenna, is studied in order to enhance the spontaneous emission (SE) rate of low emission efficiency QDs. A systematic analysis for treating the isolated nano-pillar and loose ordered pillar is demonstrated by solving the electromagnetic field equations. As an illustrative example of potential applications, we proposed a new structure that Germanium (Ge) QDs are located in close proximity to the isolated Indium Tin Oxide (ITO) nano-pillar to raise its efficiency. From the results of numerical calculation, it is predicted that ITO pillars with slim (e.g., the radius is 25 nm and the height is 500 nm) and flat morphology (e.g., the radius is 40 nm and the height is 60 nm) exhibit superior enhancement over 20 folds. Finite difference time domain (FDTD) simulation is utilized for demonstrating the distinctive enhancement when QDs radiate at surface plasmonic resonance frequency of ITO nano-pillar. It can be found that the QDs emission enhancement profile accords with our results obtained from numerical analysis.

© 2016 Optical Society of America

OCIS codes: (240.6680) Surface plasmons; (250.5403) Plasmonics; (250.5590) Quantum-well, -wire and -dot devices; (240.3990) Micro-optical devices.

References and links

1. K. Okamoto, I. Niki, A. Shvartser, Y. Narukawa, T. Mukai, and A. Scherer, "Surface-plasmon-enhanced light emitters based on InGaN quantum wells," *Nat. mater.* **3**(9), 601–605 (2004).
2. F. M. Ross, J. Tersoff, and R. M. Tromp, "Coarsening of self-assembled Ge quantum dots on Si (001)," *Phys. Rev. Lett.* **80**(5), 984 (1997).
3. A. D. Rossi, M. Carras, and D. J. Paul, "Low-Loss Surface-Mode Waveguides for Terahertz SiSiGe Quantum Cascade Lasers," *IEEE J. Quantum Elect.* **42**(12), 1233–1238 (2007).
4. C. C. Wang, H. Ku, C. C. Liu, K. K. Chong, C. I. Hung, Y. H. Wang, and M. P. Houng, "Enhancement of the light output performance for GaN-based light-emitting diodes by bottom pillar structure," *Appl. Phys. Lett.* **91**(12), 121109 (2007).
5. G. Sun, J. B. Khurgin, and R. A. Soref, "Plasmonic light-emission enhancement with isolated metal nanoparticles and their coupled arrays," *J. Opt. Soc. Am. B* **25**(10), 1748–1755 (2008).
6. R. Bose, X. D. Yang, R. Chatterjee, J. Gao, and C. W. Wong, "Weak coupling interactions of colloidal lead sulphide nanocrystals with silicon photonic crystal nanocavities near 1.55 m at room temperature," *Appl. Phys. Lett.* **90**(11), 111117 (2007).
7. J. Gersten and A. Nitzan, "Spectroscopic properties of molecules interacting with small dielectric particles," *J. Chem. Phys. J. Chem. Phys.* **75**(3), 1139–1152 (1981).

8. A. C. Pineda and D. Ronis, "Fluorescence quenching in molecules near rough metal surfaces," *J. Chem. Phys.* **83**(10), 5330–5337 (1985).
9. D. J. Griffiths, *Introduction to Quantum Mechanics* (Prentice Hall, 1995).
10. E. M. Purcell, H. C. Torrey, and R. V. Pound, "Resonance absorption by nuclear magnetic moments in a solid," *Phys. Rev.* **69**(1-2), 37–38 (1946).
11. E. Kasper, M. Oehme, J. Werner, T. Aguirov, and M. Kittler, "Direct band gap luminescence from Ge on Si pin diodes," *Front. Optoelectron.* **5**(3), 256–260 (2012).
12. K. V. Sreekanth, T. Biaglow, and G. Strangi, "Directional spontaneous emission enhancement in hyperbolic metamaterials," *J. Appl. Phys.* **114**(14), 134306 (2013).
13. S. A. Maier, *Plasmonics: Fundamental and Applications* (Springer, 2007).
14. H. T. Hattori, Z. Li, D. Liu, I. D. Rukhlenko, and M. Premaratne, "Coupling of light from microdisk lasers into plasmonic nano-antennas," *Opt. Express* **17**(23) 20878–20884 (2009).
15. R. Ruppin, "Decay of an excited molecule near a small metal sphere," *J. Chem. Phys.* **76**(4), 1681–1684 (1982).
16. L. Novotny, B. Hecht, *Principles of Nano-Optics* (Cambridge University, 2007).
17. F. Michelotti, L. Dominici, E. Descrovi, N. Danz, and F. Menchini, "Thickness dependence of surface plasmon polariton dispersion in transparent conducting oxide films at 1.55 m," *Opt. Lett.* **34**(6), 839–841 (2009).
18. J. B. Khurgin and G. Sun, "Enhancement of optical properties of nanoscaled objects by metal nanoparticles," *J. Opt. Soc. Am. B* **26**(12), 83–95 (2009).
19. G. Ritchie, E. Burstein, and R. B. Stephens, "Optical phenomena at a silver surface with submicroscopic bumps," *J. Opt. Soc. Am. B* **2**(4), 544–551 (1985).
20. J. B. Khurgin and G. Sun, "Impact of surface collisions on enhancement and quenching of the luminescence near the metal nanoparticles," *Opt. Express* **23**(24), 30739–30748 (2015).
21. W. L. Stutzman and G. A. Thiele, *Antenna Theory and Design (Third Edition)* (Wiley, 2012).
22. C. P. Huang, X. G. Yin, H. Huang, and Y. Y. Zhu, "Study of plasmon resonance in a gold nanorod with an LC circuit model," *Opt. Express* **17**(8), 6407–6413 (2009).
23. U. Laor and G. C. Schatz, "The effect of randomly distributed surface bumps on local field enhancements in surface enhanced Raman spectroscopy," *J. Chem. Phys.* **76**(6), 2888–2899 (1982).
24. C. H. Cho, C.O. Aspetti, J. Park, and R. Agarwal, "Silicon coupled with plasmon nanocavities generates bright visible hot luminescence," *Nat. Photonics*, **7**(4), 285–289 (2013).
25. C. Mayr, M. Taneda, C. Adachi, and W. Brutting, "Different orientation of the transition dipole moments of two similar Pt (II) complexes and their potential for high efficiency organic light-emitting diodes," *Org. Electron.* **15**(11), 3031–3037 (2014).
26. E. Kasper, H. J. Herzog, and H. Kibbel, "A one-dimensional SiGe superlattice grown by UHV epitaxy," *Appl. Phys.* **8**(3), 199–205 (1975).
27. Y. Huangfu, W. Zhan, X. Hong, X. Fang, G. Ding, and H. Ye, "Optimal growth of Ge-rich dots on Si (001) substrates with hexagonal packed pit patterns," *Nanotechnology* **24**(3), 635–639 (2012).
28. X. Fang, C. L. Mak, J. Dai, K. Li, H. Ye, and C. W. Leung, "ITO/Au/ITO sandwich structure for near-infrared plasmonics," *Appl. Mater. & Interfaces* **6**(18), 15743–15752 (2014).
29. G. V. Naik, V. M. Shalaev, and A. Boltasseva, "Alternative plasmonic materials: beyond gold and silver," *Adv. Mater.* **25**(24), 3264–3294 (2013).
30. M. J. Alam and D. C. Cameron, "Optical and electrical properties of transparent conductive ITO thin films deposited by sol-gel process," *Thin Solid Films* **377-378**, 455–459 (2000).
31. R. U. Tok and K. Sendur, "Absorption efficiency enhancement in inorganic and organic thin film solar cells via plasmonic honeycomb nanoantenna arrays," *Opt. Lett.* **38**(16), 3119–3122 (2013).

1. Introduction

Silicon based light source, playing a vital role in silicon integrated optoelectronic devices and chips, has been studied extensively recently [1]. Germanium, which is compatible to silicon complementary metal oxide semiconductor (CMOS) fabrication process, is an ideal material to be formed into QDs as emitters for the silicon based light source [2]. In fact, the low-radiation efficiency of Ge has been the barrier for its application while introduction of surface plasmonic enhancement for improving its efficiency may put it into practice [3]. Based on integrating certain types of nano-cavity near the pumped QDs to increase the density of states (DOS) of QDs' light field, quantum efficiency will be effectively improved, though accompanied by some radiation loss of the cavity. Over the past years, in order to achieve enhancement of efficiency, much attention has been paid to the fabrication of such nano-structures and enhancement was tested directly by experiments [4]. However, an analytic and numerical deduction of the whole physical process is overlooked more or less, which should have been emphasized equally. In

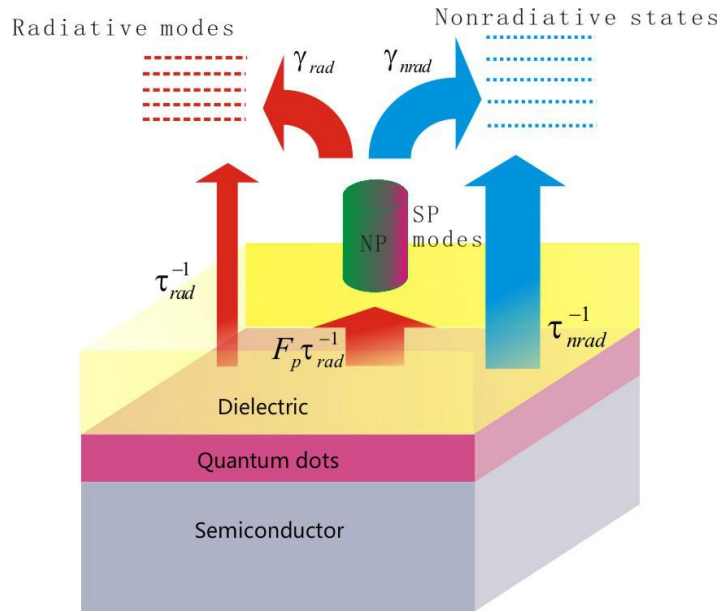


Fig. 1. Illustration of the surface plasmonic enhancement, with an isolated NP placed near a layer of active QDs in dielectric, where τ_{rad}^{-1} is the radiative decay rate of QDs, $F_p \tau_{rad}^{-1}$ is the energy transferred from emitter into SP modes, τ_{nrad}^{-1} is the nonradiative decay rate of QDs, γ_{rad} is the radiative decay rate of SPs, and γ_{nrad} is the nonradiative decay rate of SPs.

this aspect, Sun et al has made much pioneering work [5].

The whole process of surface plasmonic enhancement can be interpreted like Fig. 1. Semiconductor QDs, which generate the dipole-field, have their initial efficiency. Nevertheless, due to the influence of the proximity nano-structure, field distribution is disturbed intensely. Since the surface plasmon polariton (SPP) is induced at the metal-dielectric interface, the field is concentrated near the surface with confined large wavevector and high DOS, leading to increase of radiative recombination rate and thus the quantum efficiency of the QDs [6]. On the other hand, while the quantum efficiency of the QDs is improved, not all the energy can be coupled into free space as photons. Actually, most of it decays in nano-particles (NPs) because it could be hard for large wavevector SPP to be coupled into free space [5]. Since the NPs can efficiently transfer the electromagnetic (EM) energy from near field to far field, they can be considered as nano-antennas. Therefore, in order to calculate the total enhancement of initial efficiency, two critical parameters should be figured out, namely, SE rate enhancement and the radiative efficiency of the nano-antenna.

As for NP array shown in Fig. 2, more factors including field redistribution due to coupling between different particles, and the spectrum widening $\Delta\omega$ should be taken into account. Obviously, owing to the field coupling, confinement of field should be weaker, leading to decrease of DOS. However, these negative effects are ignored once the condition of NP loose array is satisfied. In the case of ordered loose array, the distance between neighbors should be more than twice as long as the dimension of NPs, weak coupling between neighbors could be employed to analyze the performance of single NP in array. To calculate out the spectrum widening, or the decrease of quality factor (Q factor) of the nano-cavity [7], the mathematical method similar to the one which was used to analyze periodical potential wells in quantum mechanics [8] could be

adopted. If only perturbation from nearest neighbors is considered, spectrum widening would be derived analytically.

2. Critical parameters for light emission enhancement

Since the size of the nano-cavity is much shorter than the wavelength, the static EM analysis can be applicable to the present problem of light emission enhancement. For a QD in free space, the initial efficiency is given by [9]

$$\eta_{rad} = \frac{\tau_{rad}^{-1}}{\tau_{rad}^{-1} + \tau_{nrad}^{-1}}, \quad (1)$$

where τ_{rad} and τ_{nrad} represent radiation lifetime and the non-radiation lifetime of electron-hole pairs, respectively. In view of the fact that τ_{rad} is much longer than τ_{nrad} , the equation can be simplified as

$$\eta_{rad} = \frac{\tau_{rad}^{-1}}{\tau_{nrad}^{-1}}. \quad (2)$$

Several forms of non-emission recombination exist [10, 11], including auger recombination and those transmitted energy as phonons, which are not likely to be affected by the change of modes of emitted photons, so that τ_{nrad} tends to be constant. On the other hand, according to the Fermi golden rule, the SE probability has a form as [12]

$$\eta_{ij} = |M_{ij}|^2 \rho, \quad (3)$$

where η_{ij} is the electron transition rate from energy level $|i\rangle$ to $|j\rangle$, M_{ij} is the dipole matrix, whose elements are the quantum constants for a certain QD, relating two energy levels, and ρ is the DOS of the emitter, such as QD. M_{ij} has the form of $\langle i|e\mathbf{r}|j\rangle$, where e and \mathbf{r} denote the charge and the displacement vector, respectively, of carriers in a QD ($\langle i|$ is the Hermitian conjugate of the energy state $|i\rangle$ of the carriers in the QD). It is apparent that only the term ρ can be changed within the size, which differs in the range of 10^{-8} m. Assuming only one mode can exist at cavity resonance, in the spectral domain, the DOS in the cavity ρ_{sp} can be presented as [13]

$$\rho_{sp} = \frac{1}{V_{eff}\Delta\omega}. \quad (4)$$

The effective mode volume V_{eff} is used as the ratio of the total SPP mode to the energy density at the position of highest field E_{max} , which can be used to qualify the strength of light-matter interactions in cavity [13]. After integrating the energy density over the whole space, the energy U , a significant part of which is concentrated in the nano-cavity, turns out to be

$$U = 0.5\epsilon_0\epsilon_d E_{max}^2 V_{eff}, \quad (5)$$

and the effective mode volume of the cavity V_{eff} is thus given by

$$V_{eff} = \frac{\int_{in} 0.5\epsilon_0 \frac{\partial\omega\epsilon_M}{\partial\omega} E^2 dV + \int_{out} 0.5\epsilon_0\epsilon_d E^2 dV}{0.5\epsilon_0\epsilon_d E_{max}^2}, \quad (6)$$

where ϵ_d is the permittivity of the surrounding dielectric, ϵ_M is the Drude-model permittivity for plasmonic material and E is the electric field in the space [5]. Based on the Drude model, the metal dispersion ϵ_M is written as [13]

$$\epsilon_M = 1 - \frac{\omega_p^2}{\omega^2 + i\nu\omega}, \quad (7)$$

where ω_p is the plasma frequency and v is plasmonic material's loss. Frequency ω should be at the value where the maximum field occurs. And at this value stimulated SPP field is much more intense than the stimulating field. The effective mode volume of quantum dots (V_{eff-qd}) could be obtained from V_{eff} by

$$V_{eff-qd} = V_{eff} \left(\frac{E_{max}}{E_{QD}} \right)^2, \quad (8)$$

where E_{QD} is the electric field at the position of the QD. To calculate the V_{eff-qd} , the relationship between field intensity at the surface of the cavity and that at the QD needs to be evaluated.

On the other hand, energy loss in the cavity, which cannot be coupled to free space, can be calculated as

$$\left(\frac{dU}{dt} \right)_{nrad} = \int_{in} \frac{1}{2} \epsilon_0 \text{Im} \left(\frac{\partial \omega \epsilon_M}{\partial \omega} \right) \omega E^2 dV. \quad (9)$$

Meanwhile, the energy coupled into free space can be calculated through closed surface integral of Poynting vector from the cavity. Once the cavity is identified as an antenna, its radiation rate can be calculated by using its polarization momentum [14]. So the emitted power has the form

$$\left(\frac{dU}{dt} \right)_{rad} = \oint \vec{S} \cdot d\vec{s}. \quad (10)$$

The Poynting vector $\langle S \rangle$ is given by

$$\langle S \rangle = \frac{1}{2} \text{Re}[\vec{E} \times \vec{H}^*] = \frac{1}{2} \vec{r}_0 \sqrt{\frac{\mu_0}{\epsilon_0 \epsilon_d}} \left| \frac{k_d \omega_p}{4\pi r} \right|^2 \sin^2(\theta), \quad (11)$$

where k_d is the wavevector in the dielectric, \vec{r}_0 is the unit position vector, r is the distance from the position to the origin, and θ is the altitude angle. The radiated power can therefore be written as

$$P_r = \int_0^{2\pi} d\phi \int_0^\pi d\theta r^2 \sin\theta \langle S \rangle = \frac{\omega^4 \epsilon_d^{1.5}}{12\pi \epsilon_0 c^3} |p|^2, \quad (12)$$

where p is the total polarized momentum of the NP and ϕ is the azimuth angle. The power decay rate γ is

$$\gamma = \frac{\left(\frac{dU}{dt} \right)_{rad} + \left(\frac{dU}{dt} \right)_{nrad}}{U}. \quad (13)$$

The Fourier spectrum for the radiation wavelength is $\frac{2}{\pi\gamma} \frac{\gamma^2/4}{\gamma^2/4 + (\omega - \omega_0)^2}$, which has the form of Lorentzian line shape. We might as well suppose the line width can be presented as

$$\Delta\omega = (\pi/2)\gamma. \quad (14)$$

As a result, the Q factor is [9]

$$Q = \omega_0 / \Delta\omega, \quad (15)$$

where ω_0 represents surface plasmonic resonance frequency. In the free space, when the fixed polarization is taken into consideration, the DOS of the QD is equal to [13]

$$\rho_{rad} = \frac{1}{3\pi^2} \left(\frac{2\pi}{\lambda_d} \right)^3 / \omega_0, \quad (16)$$

where λ_d is the emission wavelength in the dielectric. When NP is placed nearby, the DOS is enhanced by Purcell factor F_p , which can be expressed as

$$F_p = \frac{3}{8\pi} \lambda_d^3 \frac{Q}{V_{eff-qd}}. \quad (17)$$

As a result, the SE rate of QDs becomes [8]

$$\frac{1}{\tau'_{rad}} = \frac{F_p}{\tau_{rad}}. \quad (18)$$

However, while the efficiency of QD rises, loss caused by the plasmonic material particle plays a vital role. The radiation efficiency of the particle η_r could be defined as the ratio of radiation decay rate to the total energy decay rate. That is,

$$\eta_r = \frac{\gamma_{rad}}{\gamma_{rad} + \gamma_{nrad}}, \quad (19)$$

which is a very small value. Now, with the existence of nearby NP, the total SE efficiency η_{sp} becomes

$$\eta_{sp} = \frac{\tau_{rad}^{-1}(1+F_p\eta_r)}{\tau_{nrad}^{-1} + \tau_{rad}^{-1}(1+F_p)}. \quad (20)$$

So the whole enhancement can be approximately written as $1+F_p\eta_{sp}$, under the condition that the initial SE of emitter is extremely low. Even though η_r is small, namely SPP loss overwhelms radiation, the SE efficiency is amplified by a much larger value F_p , and so it is worth using these cavities for enhancement, particularly for QD with low SE efficiency, like the indirect bandgap type Ge QDs whose efficiency will dramatically increase [15]. The whole processes can be interpreted vividly by Fig. 1.

It is impossible to deduce the fine frequency broadening due to cavities' coupling. However, when a perturbing field from the neighbor NP is much weaker than NP's own field, like less than 20% of the internal field, the perturbation model could be used, which only considers the four neighbor particles. Assume the field of an isolated pillar has the form $\vec{E}(\vec{r})e^{j\omega t}$. In an ordered array as Fig. 2, the distance between each nano-pillar is b . Note that the coupling makes the field split. The field can be written as $\sum \omega_{m,n}(t)E(\vec{r})$, where $\omega_{m,n}(t) = C_{m,n}e^{j\omega t}$. As a result of the periodicity of the array, $C_{m,n}$ is also periodic, i.e., $C_{m,n} = ke^{j(bm+bn)}$. Since the operator $\frac{\partial^2}{\partial r^2}$ is equivalent to $-\omega^2$, substituting the form of the solution into Maxwell equation, [16]

$$\Delta \vec{E} = \epsilon\mu \frac{\partial^2}{\partial t^2} \vec{E}, \quad (21)$$

we can obtain

$$\begin{aligned} \omega^2 = \omega_0^2 \left[1 + \frac{E_{m,n-1,out}}{E_{in}} \cos(bX_n) + \frac{E_{m,n+1,out}}{E_{in}} \cos(bX_n) + \right. \\ \left. \frac{E_{m-1,n,out}}{E_{in}} \cos(bX_m) + \frac{E_{m+1,n,out}}{E_{in}} \cos(bX_m) \right], \end{aligned} \quad (22)$$

where X is the wavenumber of SPP-Bloch wave (SPP-BW). Spectrum is thus broadened. Generally speaking, the wavevector of the space period structure which is related to SP is larger than the wavevector of photons in the dielectric, and the reasonable extent for the wavevector of SP that can be coupled out should have $\sqrt{X_m^2 + X_n^2} < k_d$, where k_d is regarded as space

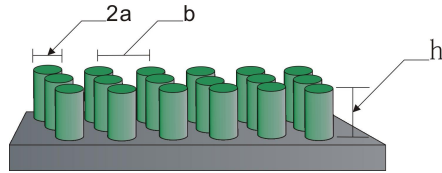


Fig. 2. Illustration of a pillar ordered array, where a and h represent the radius and the height, respectively, of the pillar, and b is the center-to-center spacing between two neighboring pillars.

period vector. Additionally, we need to do modification to the radiation decay rate γ_{rad} , since only partition of the SPP modes whose value of wavevector is smaller than k_d can be coupled out [17]. It can be seen that the non-ordered array can be a good solution for overcoming this negative influence thanks to decoupling. The looser the array, the weaker the enhancement for those QDs far from the pillars, and the lower the DOS that the pillar can supply.

3. Numerical calculation and analysis for enhancement

Traditionally, among most of references about using micro-structure to enhance light emission, analytic results usually focus on spherical cavity or bumps on a plasmonic material's surface, like Jacob Khurgin's work [18] and many famous papers [19] about Surface Enhanced Raman Scattering (SERS). The field will be intensive over high curvature positions, so spheres with small radius lead to high DOS. However, based on those references, it can be found that, compared with those shapes with low symmetry, the enhancement for spherical cavity is much more dimensionally sensitive, leading to great challenges in device fabrication process, calling for sophisticated fabrication. Other shapes can avoid this problem, like pillar or inverted cone. Moreover, compared with the spherical NP configuration, the pillar has more alterable variables, including the radius and height, both of which are tunable to gain smaller V_{eff} and to achieve higher enhancement. Furthermore, another merit of the pillar shape is that the enhancement is less sensitive to radiative frequency compared to the spherical cavity, which enables the similar enhancement even with some broadening of the source. Inverted cone, along with some similar structures, is also apparently more flexible than spheres. More importantly, owing to a little bit lower Q factor and much smaller V_{eff} , the inverted cones perform even better than pillars, as the result that antenna radiative efficiency is inversely proportional to Q, and F_p is inversely proportional to V_{eff} . Nevertheless, analytical calculation for inverted cone is almost impossible, and the fabrication for the structure with a tiny point is quite difficult for the present. This is the reason for why nano-pillars are chosen in this work.

Some conclusions from previous work are constructive [5, 18, 20]. Typically, tightly confined energy with large wavevector is relatively difficult to be coupled into free space from SPP mode, and they also suffer from large loss due to field penetration into the plasmonic material. Actually, those tightly confined modes belongs to high order modes. So those references [5, 21] tell us about how to calculate and cancel those high order modes. Since sphere is extremely symmetrical, it is much easier to be analyzed than those shapes, e.g., pillars. Therefore, in the following case, the enhancement should be calculated in such a special way [22].

It is well known that there are two kinds of polarization dominating in the distribution of elec-

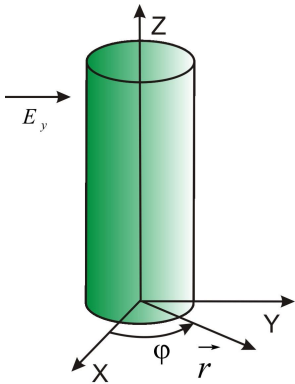


Fig. 3. Illustration of the nano-pillar with a stimulating electric field of horizontal polarization, where ϕ is the angle between the position vector \mathbf{r} and the x-axis.

tromagnetic (EM) field, namely, the horizontal polarization whose electric field is perpendicular to the pillar and the vertical polarization with the electric field along the pillar. It is difficult to evaluate the exact field distribution due to the complex boundary conditions, let alone the SE rate of each QD, which varies from one another, is not known before our calculation. Here we try to treat the two polarized electric fields independently, the process of calculation is therefore simplified, and hence it is possible for us to obtain the explicit theoretical formalisms for these two cases (horizontal and vertical polarizations).

3.1. The horizontal polarization

When the polarization of electric field is vertical to the central axis of pillar, the electromagnetic modes on the pillar can be stimulated by the incident plane wave from bottom to up, as shown in Fig. 3. While the ideal transverse electromagnetic wave (TEM) is absent in such a pillar, the quasi TEM analysis for the electric field is suitable, assuming the wavevector is along the axis.

Above all, plasmonic resonance frequency should be figured out. As the length of the pillar is several times larger than its radius, the variation of field along the axis is much less than that along the radius. At the optical communication spectrum, based on the fact that the wavelength and the skin depth are much larger than the geometric size of the nano-pillar, the quasi-static analysis can be utilized as phase change in the pillar can be ignored. Therefore, the electric potential satisfies the Laplace equation

$$\Delta\Phi = \frac{1}{r} \left(\frac{1}{r} \frac{\partial^2}{\partial\phi^2} + \frac{\partial}{\partial r} \left(r \frac{\partial}{\partial r} \right) \right) \Phi = 0, \quad (23)$$

of which the solution reads

$$\Phi = C \ln r + B + \sum_{-\infty, n \neq 0}^{\infty} r^n (A_n \cos n\phi + B_n \sin n\phi). \quad (24)$$

According to the boundary conditions (i.e., the field is finite inside the pillar, and the electric displacement vector in the normal direction is continuous across the surface), the solution can be obtained:

$$\Phi_{inside} = \left(\frac{-2\epsilon_d}{\epsilon_M + \epsilon_d} \right) r \cos \phi, \quad (25)$$

$$\Phi_{outside} = \left[\left(\frac{\epsilon_M - \epsilon_d}{\epsilon_M + \epsilon_d} \right) \frac{a^2}{r} - r \right] \cos\phi. \quad (26)$$

The stimulated SPP mode should be much more intensive than the stimulating field. Using the formula for the real part of the dielectric constant of plasmonic material in the Drude model, $\epsilon_M = 1 - \frac{\omega_p^2}{\omega^2}$, the resonance frequency should be

$$\omega = \sqrt{\frac{\omega_p^2}{1 + \epsilon_d}}, \quad (27)$$

where ω_p is the electron plasma frequency, and ω is the frequency of the optical field. Actually, from the transition of SPP to the localized surface plasmon (LSP), namely different modes,

plasmonic resonance frequency will change from $\sqrt{\frac{\omega_p^2}{1 + \epsilon_d}}$ to $\sqrt{\frac{\omega_p^2}{1 + 2\epsilon_d}}$ [5, 12]. In a specific

case, when an ITO pillar with ω_p of 2.2×10^{15} rad/s, stands on the surface of a thick silicon dioxide (SiO_2) film with permittivity of 2.1, the frequency for maximum efficiency enhancement is around 1550 nm, the central frequency of C-band for optical communication, which can be chosen as plasmonic resonance frequency. Then the electric field, which is the gradient of the above potential functions, is given by

$$E_r = \begin{cases} \left(\frac{\epsilon_M - \epsilon_d}{\epsilon_M + \epsilon_d} - 1 \right) \cos\phi & r < a \\ - \left(\frac{\epsilon_M - \epsilon_d}{\epsilon_M + \epsilon_d} \frac{a^2}{r^2} + 1 \right) \cos\phi & r > a \end{cases}, \quad (28)$$

$$E_\phi = \begin{cases} \left(\frac{\epsilon_M - \epsilon_d}{\epsilon_M + \epsilon_d} - 1 \right) \sin\phi & r < a \\ \left(\frac{\epsilon_M - \epsilon_d}{\epsilon_M + \epsilon_d} \frac{a^2}{r^2} - 1 \right) \sin\phi & r > a \end{cases}. \quad (29)$$

If we do not suppose that the length is large, the Maxwell equation should be solved in this form, $(\nabla^2 + \epsilon \mu \omega^2) E_y$, namely, $(\nabla^2 + \epsilon_r k_0^2) E_y$, where ϵ_r is the relative permittivity. We assume the electric field in the y-direction

$$E_y = R(r)\Phi(\phi)e^{-jk_z z}, \quad (30)$$

where k_z is the wavevector along the axis. With the help of the boundary conditions, we can have

$$E_y = \begin{cases} D \frac{J_n(k_{l1}r)}{J_n k_{l1} a} \cos n\phi e^{-jk_z z} & r < a \\ D \frac{K_n(k_{l2}r)}{K_n k_{l2} a} \cos n\phi e^{-jk_z z} & r > a \end{cases}, \quad (31)$$

where J_n , K_n are the first and second kinds of Bessel functions, respectively. The undetermined parameters k_{l1} , k_{l2} , k_z have the relationship:

$$k_{l1}^2 = \left(\frac{2\pi}{\lambda_0} \right)^2 \epsilon_M - k_z^2, \quad (32)$$

$$k_{l2}^2 = \left(\frac{2\pi}{\lambda_0} \right)^2 \epsilon_d - k_z^2, \quad (33)$$

$$\frac{k_{t1}J_{n-1}(k_{t1}a)}{\sqrt{\epsilon}J_n(k_{t1}a)} = \frac{k_{t2}J_{n-1}(k_{t2}a)}{\sqrt{\epsilon}J_n(k_{t2}a)}, \quad (34)$$

which should be complex numbers. So we can obtain the magnetic field and thus electric field along the axis, and the results are given by

$$H_x = -\frac{E_y}{\sqrt{\mu/\epsilon_0\epsilon}}, \quad (35)$$

$$E_z = \frac{-j}{\omega\epsilon} \left(\frac{\partial H_y}{\partial x} - \frac{\partial H_x}{\partial y} \right) \approx \frac{j}{\omega\epsilon} \frac{\partial H_x}{\partial y}. \quad (36)$$

It should be noted that the high order modes with the form of Legendre functions were excluded in Jacob Khurgin's work with sphere cavity [19] because the multi-dipoles can cancel each other out and hence the high order modes cannot be coupled into the free space. This can also be explained within the framework of wave theory: specifically, the high order modes have tightly confined fields over surface (and hence large wavevectors). This leads to failure in phase matching, and the high order modes cannot be coupled out as emitted photons. In a pillar cavity, all orders have the form of Bessel functions, and it is easy to see that high order Bessel functions are also confined near the surface of the pillar. So in some coarse approximation, the high order components are ignored, and then the field can be written as

$$E_y = \begin{cases} D \frac{J_0(k_{t1}r)}{J_0 k_{t1} a} \cos n\phi e^{-jk_z z} & r < a \\ D \frac{K_0(k_{t2}r)}{K_0 k_{t2} a} \cos n\phi e^{-jk_z z} & r > a \end{cases}. \quad (37)$$

As far as how to analyze the high order modes is concerned, we will refer to Gersten and Nitzan's work [5], where the high-order coefficients in series solutions have been determined. In the simplified expressions (28) and (29) for the fields inside and outside the pillar, we shall add the phase factor $e^{jk_M z}$, with

$$k_M = \frac{\omega}{c} \sqrt{\epsilon_M}, \quad (38)$$

where $\epsilon_M = -\epsilon_d$, namely, $k_M = jk_d$. The whole energy formula and the field are obtained

$$\begin{aligned} U &= \frac{(3 + \epsilon_d)\epsilon_0 E_{max}^2 (1 - e^{-2k_d h}) \pi a^2}{4k_d} \\ &= 0.5\epsilon_0\epsilon_d E_{max}^2 V_{eff}, \end{aligned} \quad (39)$$

$$V_{eff} = \left(1 + \frac{3}{\epsilon_d}\right) \frac{1 - e^{-2hk_d}}{2hk_d} \pi a^2 h. \quad (40)$$

On the other hand, the polarization momentum is given by

$$p = \int \vec{P} dV = \int_0^l \frac{-2\epsilon_0\epsilon_d(-\epsilon_d - 1)}{\epsilon_M + \epsilon_d} E_0 \pi a^2 e^{jk_d z} dz. \quad (41)$$

The emitted power is of the form

$$\begin{aligned}
P_r &= \int_0^{2\pi} d\phi \int_0^{2\pi} d\theta r^2 \sin\theta \langle S \rangle \\
&= \frac{\omega^4 \epsilon_d^{1.5}}{12\pi \epsilon_0 c^3} |p| \\
&= \frac{\omega^4 \epsilon_d^{1.5} (\pi a^2 h)^2 (1 + \epsilon_d)^2}{12\pi \epsilon_0 c^3} \left(\frac{1 - e^{-hk_d}}{hk_d} \right)^2 E_{max}^2 \\
&= \left(\frac{dU}{dt} \right)_{rad},
\end{aligned} \tag{42}$$

and the energy decay rate in the pillar turns out to be

$$\left(\frac{dU}{dt} \right)_{nrad} = v(1 + \epsilon_d) \pi a^2 h E_{max}^2 \frac{1 - e^{-2k_d h}}{2k_d h}. \tag{43}$$

When the wavelength is longer than four times the length of the pillar, we have the total decay rate

$$\gamma = \frac{v(1 + \epsilon_d) + \frac{\omega_0^4 \epsilon_d^{1.5} a^2 h}{12c^3} (1 + \epsilon_d^2)}{0.5(3 + \epsilon_d)}. \tag{44}$$

The radiation efficiency of the pillar is

$$\eta_r = \frac{\frac{\omega_0^4 \epsilon_d^{1.5} a^2 h}{12c^3} (1 + \epsilon_d)}{v + \frac{\omega_0^4 \epsilon_d^{1.5} a^2 h}{12c^3} (1 + \epsilon_d)}. \tag{45}$$

When the change rate of the field intensity outside the pillar is taken into account, the effective mode volume of a quantum dot is given by

$$V_{eff-qd} = V_{eff} \left(\frac{h+d}{h} \right)^4, \tag{46}$$

where d is the distance from QD to the bottom of the pillar. By using all the above results, the enhancement factor, which has been defined in Eq. (17), can be written in the form

$$F_p = \frac{6c^3 (1 + \epsilon_d) k_d}{\epsilon_d^{0.5} \omega_p^2 \left(v + \frac{\omega_0^4 \epsilon_d^{1.5} a^2 h}{12c^3} \right) (1 - e^{-2hk_d}) a^2} \left(\frac{h}{h+d} \right)^4. \tag{47}$$

Now the total enhancement factor is

$$F_{single} = \frac{(1 + \epsilon_d) k_d \epsilon_d h \omega_o^2}{2 \left(v + \frac{\omega_0^4 \epsilon_d^{1.5} a^2 h}{12c^3} \right)^2 (1 - e^{-2hk_d})} \left(\frac{h}{h+d} \right)^4 + 1. \tag{48}$$

The total enhancement factor F_{single} exhibits a strong dependence on the size of plasmonic material nano-pillar as shown in Fig. 4, when the polarized direction of electric field is vertical

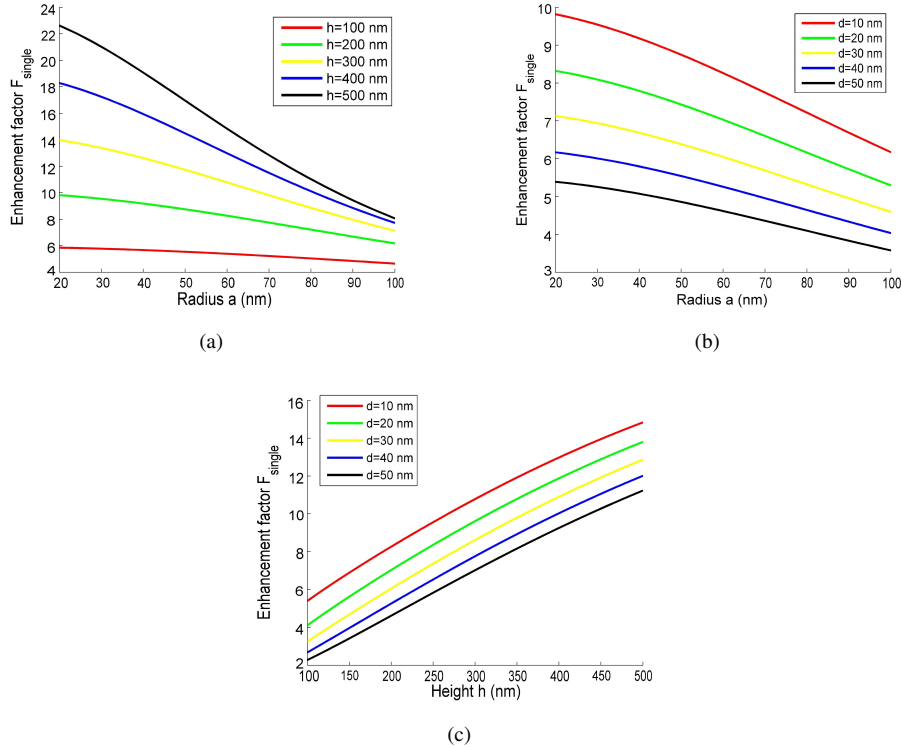


Fig. 4. Enhancement factor F_{single} (due to a single isolated ITO pillar with the electric field of a horizontal polarization) as a function of the pillar radius a and the height h . In (a), the pillar height ranges from 100 to 500 nm, and the distance d from QD to the bottom of the pillar is 10 nm; In (b), the distance d from QD to the pillar bottom ranges from 10 to 50 nm, and the pillar height h is 200 nm; In (c), the distance d from QD to the pillar bottom ranges from 10 to 50 nm and the radius a of the pillar is 60 nm.

to the axis, where ITO nano-pillar with a given loss v of $0.2\omega_p$ is used for example and the dielectric is silicon dioxide. The parameters used for numerical calculation are presented in Table. 1. The enhancement of efficiency decreases rapidly with the increase of radius of pillar and the distance from QD to the bottom of the pillar, but increases when the height of the pillar rises. These facts indicate that the leptosomatic pillar favors the higher enhancement when the horizontal polarization is applied.

Table 1. Typical Parameters of Numerical Calculation for Enhancement Factor

ω_0 (Rad/s)	ω_p (Rad/s)	v (Rad/s)	ϵ_d
1.22×10^{15}	2.2×10^{15}	4.4×10^{14}	2.1

3.2. The vertical polarization

The vertical polarization has the configuration as shown in Fig. 5, where the field is along the z-axis of the pillar. We assume the electric field has the form $E_z(r, \phi, z) = R(r)\Phi(\phi)e^{ik_M z}$. By

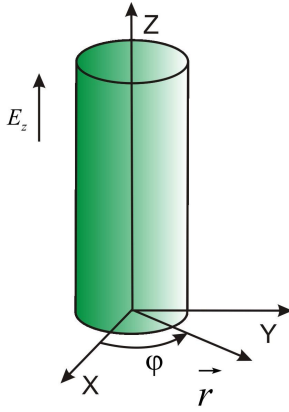


Fig. 5. Illustration of the nano-pillar with the electric field of a vertical polarization, where ϕ is the angle between the position vector \mathbf{r} and the y-axis.

solving the Maxwell equation with boundary conditions, we can obtain the solution

$$E_z = \begin{cases} J_0(k_{t1}r)e^{-\gamma_z z} & r < a \\ K_0(k_{t2}r)e^{-\gamma_z z} & r > a \end{cases} \quad (49)$$

with the relationship of the parameters k_{t1} , k_{t2} , γ_z :

$$\frac{k_{t1}}{\epsilon_M} \frac{J_0(k_{t1}a)}{J_1(k_{t1}a)} = -\frac{k_{t2}}{\epsilon_d} \frac{K_0(k_{t2}a)}{K_1(k_{t2}a)}, \quad (50)$$

$$k_{t2}^2 = k_d^2 + \gamma_z^2, \quad (51)$$

where γ_z is the decay rate along the z-axis. The present nano-pillar can be treated as a short antenna, so that the electric field far from the pillar can be written as

$$E_\phi = \int_0^h j \frac{\eta_0 k_d J(z)}{4\pi r} \sin(\phi) e^{-jk_d r + jk_d z \cos(\phi)} dz, \quad (52)$$

where J is the current and η_0 is the intrinsic impedance of the free space. The emitted power can be of the form

$$P_r = \frac{a(\pi \epsilon_0 k_d e^{-k_{t2}a})^2}{32 k_{t2} \omega^2} \int_0^\pi \sin^3(\phi) \left(\frac{e^{-jk_d r + jk_d z \cos(\phi)} - 1}{-\gamma_z + jk_d \cos(\phi)} \right)^2 d\phi. \quad (53)$$

Based on the property of Bessel functions, we can find that when $k_{t2}a < 5$, $\int_{k_{t2}a}^\infty x K_0^2(x) dx \approx 0$, namely, the energy is concentrated in the cavity. Then the whole energy is approximately given by

$$U = \pi \epsilon_0 \frac{1 - e^{-2\gamma_z h}}{2\gamma_z} (2 - \epsilon_d) \frac{a^2}{2} [I_0^2(ak_{t1}) - I_1^2(ak_{t2})]. \quad (54)$$

The effective mode volume V_{eff} and the energy decay in the pillar are given by

$$V_{eff} = \pi a^2 h \frac{2 - \epsilon_d}{\epsilon_M} \frac{1 - e^{-\gamma_z h}}{2\gamma_z h} \left[1 - \frac{I_1^2(ak_{t1})}{I_0^2(ak_{t1})} \right], \quad (55)$$

and

$$\left(\frac{dU}{dt} \right)_{nrad} = 2\pi\epsilon_0(1 + \epsilon_d)v \frac{1 - e^{-2\gamma_z h}}{2\gamma_z} \cdot \frac{a^2}{2} (I_0^2(ak_{t1}) - I_1^2(ak_{t1})), \quad (56)$$

respectively. The total decay rate and the radiation efficiency of the pillar should take the form

$$\gamma = \frac{P_r + \left(\frac{dU}{dt} \right)_{nrad}}{U}, \quad (57)$$

$$\eta_r = \frac{P_r}{P_r + \left(\frac{dU}{dt} \right)_{nrad}}, \quad (58)$$

respectively. Therefore, the Purcell factor F_p turns out to be of the form

$$F_p = \frac{\lambda^3}{4\pi^3 \gamma} \omega_0 \frac{\epsilon_d}{2 - \epsilon_M} \frac{a^2}{(a+d)^4} \cdot \frac{I_0^2(ak_{t1})}{I_0^2(ak_{t1}) - I_1^2(ak_{t1})} \frac{2\gamma_z}{1 - e^{-2\gamma_z h}}. \quad (59)$$

As a result, the enhancement could be expressed as

$$F_{single} = 1 + F_p \eta_r. \quad (60)$$

Now take the ITO nano-pillar for example again. When the electric field is vertically polarized, the enhancement factor F_{single} exhibits the same order of magnitude as that shown in Fig. 4, where the electric field is horizontally polarized (schematically shown in Fig. 6). Although, similarly, the factor F_{single} decreases when the distance from QD to the bottom of the pillar increases, and there is an optimal enhancement when the radius changes from 20 nm to 100 nm. More importantly, unlike the scenario of horizontal polarization, the enhancement factor F_{single} decreases with the increase of height of the pillar. All the facts suggest that in this situation, a flat pillar would be a better choice for higher enhancement.

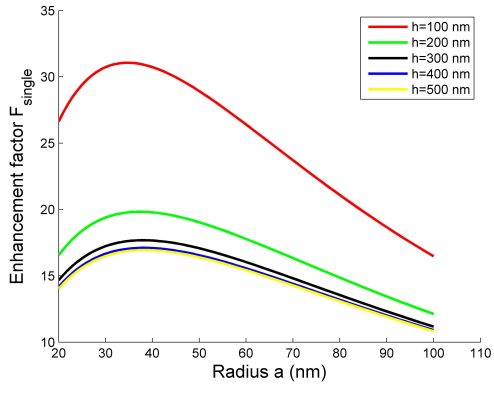
3.3. Numerical analysis for the effects of multi-cavity

Here, the electric field of pillar is applied (as an example to illustrate the weak coupling, the horizontally polarized electric field is assumed). Notice that the field outside the pillar decreases with the increase of distance quadratically. By substituting the electric field outside the pillar into the frequency broadening formula Eq. (22), we can obtain

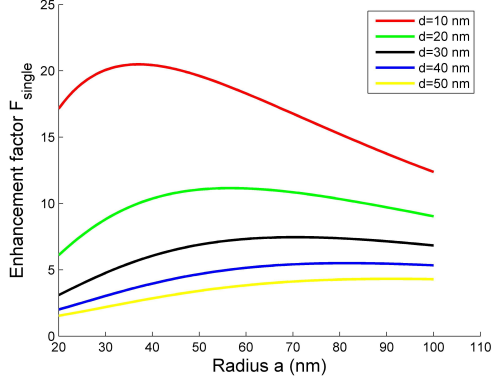
$$\omega^2 = \omega_0^2 \left[1 + 2 \left(\frac{a}{a+b} \right)^2 \right] [\cos(bX_n) + \cos(bX_m)]. \quad (61)$$

The spectrum broadening can be given by

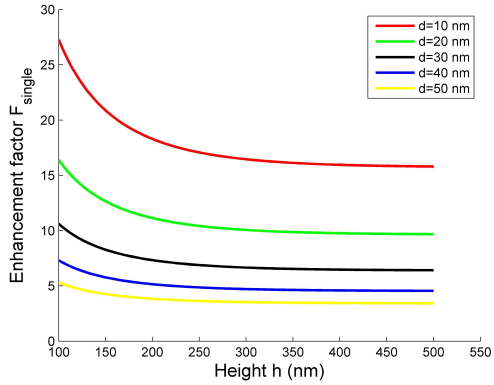
$$\left(\omega_0 \sqrt{1 + 4 \left(\frac{a}{a+b} \right)^2 \cos \left(\frac{\sqrt{2}}{2} b k_d \right)}, \quad \omega_0 \sqrt{1 + 4 \left(\frac{a}{a+b} \right)^2} \right). \quad (62)$$



(a)



(b)



(c)

Fig. 6. Enhancement factor F_{single} (due to a single isolated ITO pillar with the electric field of vertical polarization) as a function of the pillar radius a and the height h . In (a), the height ranges from 100 to 500 nm, and the distance d from QD to the pillar bottom is 10 nm; In (b), the distance d from QD to the bottom of the pillar ranges from 10 to 50 nm, and the height of the pillar is 200 nm; In (c), the distance d from QD to the pillar bottom ranges from 10 to 50 nm, and the radius of the pillar is 60 nm.

If we assume the diameter of the pillar is less than 0.3 times as long as the length, the approximate expression for the broadening due to the coupling is

$$\Delta\omega' = \frac{2}{\sqrt{1+\epsilon_d}} \left(\frac{a}{a+b} \right)^2 (1 - \cos \sqrt{2} b k_d) \omega_p. \quad (63)$$

Once plasmonic material's loss v is 10% of ω_p , widening due to the isolated cavity Q factor is around $\frac{0.1\omega_p\pi(1+\epsilon_d)}{3+\epsilon_d}$. In order that the pillar is accessible to fabrication, we assume $a = 50$ nm and b is larger than 150 nm. The coupling of ordered array only broadens $0.02\omega_p$ in frequency, which can be ignored compared with the broadening by the cavity itself. Meanwhile, the majority of power is gathered in the pillar, and so the change of field intensity inside the pillar on account of the neighbors would also be negligibly small. Thus, loose coupling can be ignored, particularly in a disordered array [23].

4. Simulation result

The theoretical model in Section 3 is established based on some ideal but unrealistic assumptions about polarizations, the obtained results would be applicable only under certain circumstances. In a real case, the electric field is always consisted of both the two polarized states. However, the proportion of the two polarized components is still unknown. Fortunately, taking advantage of FDTD (finite difference time domain) simulation, much more precise results could be reached [24].

It should be noticed that different orientations of dipoles will influence the proportion of the above two polarized states in a real electric field [25]. Here, two kinds of typical cases are discussed, namely, horizontal orientation and vertical orientation as shown in Fig. 7(a) and Fig. 7(b), respectively. Different from the concept of polarization, orientation refers to the oscillation direction of dipole in this paper. The dipoles' orientation is mainly determined by the pumping manner, as well as QDs morphology, and the horizontal one dominates once QDs are pumped with bottom-up incident light [26, 27].

Now again as an illustrative example, Indium Tin Oxide will be utilized as a nano-pillar, which has potential applications in SPP enhancement [28] in infrared range around 1550 nm [29]. In our model, a single ITO nano-pillar is standing on the surface of silicon dioxide layer. And the dipole is right under the bottom of the pillar. In the simulation, the boundary condition is set as a perfectly matched layer, and the mesh is chosen as 2 nm, which is small enough to obtain the precise distribution of the electric field. Fig. 7 shows the distribution of electric field, under the conditions of the two kinds of dipole orientations mentioned above. It is noteworthy that the electric field is localized at the border of the pillar, especially on the edge. Outside the pillar, the field decays fiercely. It is shown that the vertically orientated dipoles stimulate substantially more intensive field inside the nano-pillars than the horizontally orientated dipoles do.

Here, the enhancement with vertically oriented QD dipole is presented as Fig. 8. Once the dipole is oriented vertically, the profile of the enhancement of the ITO pillar, as the function of radius a and height h , could be explained, if the two kinds of polarizations of electric fields are taken into account. To achieve the higher enhancement, pillar with smaller radius is needed, which is also favored by the result of two polarized states. Besides, both high pillar (indicated by horizontally polarized assumption) and short pillar (indicated by vertically polarized assumption), exhibit superior enhancement factor F_{single} . In a word, both slim and flat configurations of ITO pillars are suitable for surface plasmonic enhancement, up to 22 and 25 folds, respectively, with a single QD. As a matter of fact, several QDs can also be located under one pillar. The efficiency of these QDs, accompanied by their mutual coupling, would be affected differently by

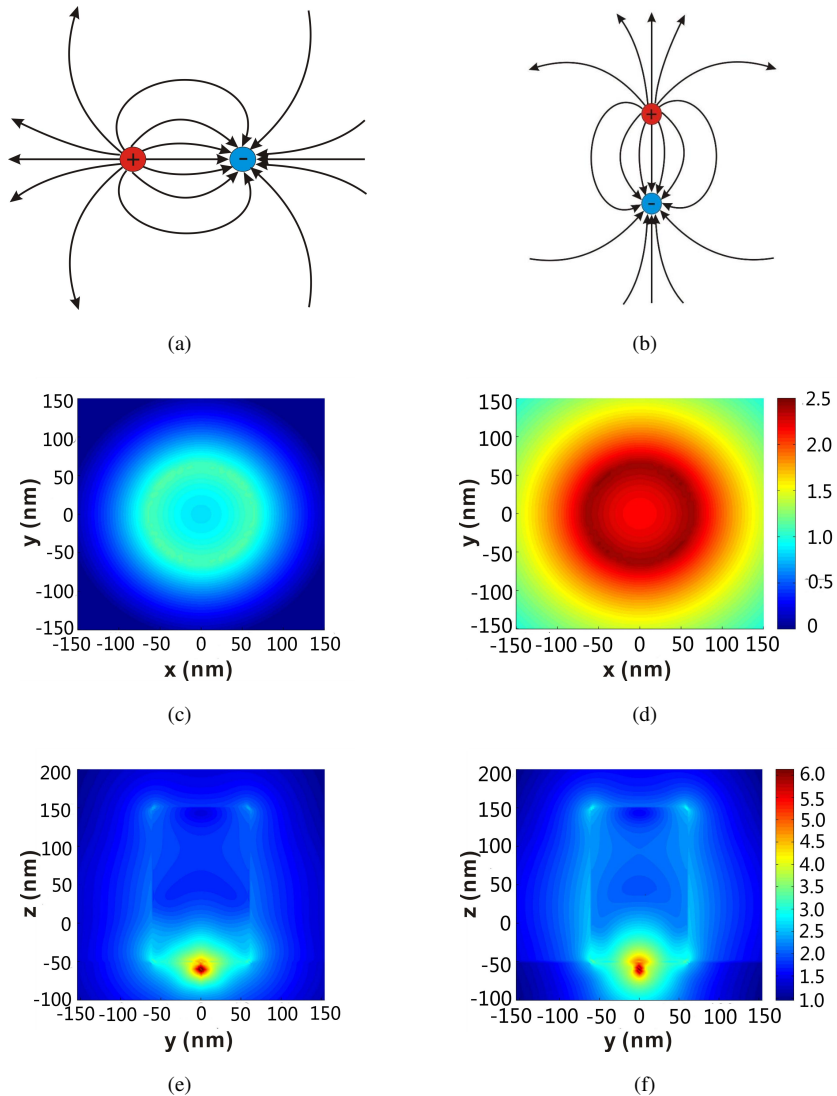
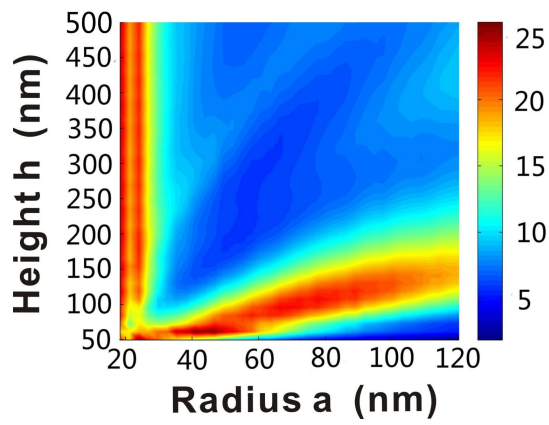
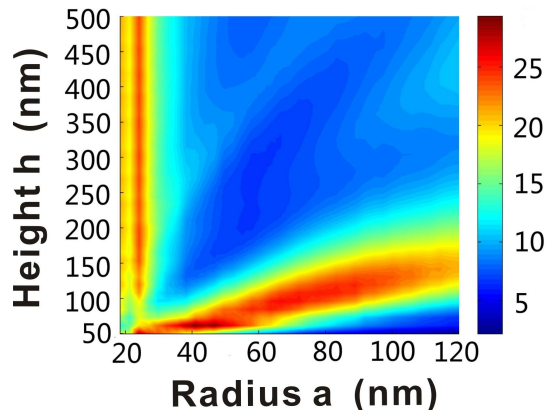


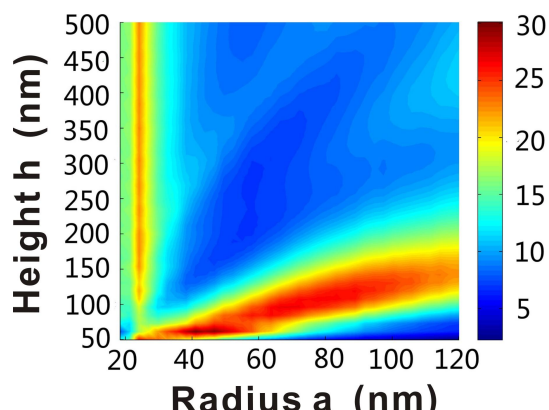
Fig. 7. The field distribution of the ITO pillar. (a) and (b) are the illustrations of the dipoles with two orientations: (a) oriented horizontally and (b) oriented vertically; (c) and (d) show the common logarithm, ($\lg |E|$), of the near field profiles of the silicon based light source with enhancement by ITO pillar. These are the top views of near-field profiles of the horizontally oriented dipole (c) and the vertically oriented dipole (d); (e) and (f) indicate the common logarithm, ($\lg |E|$), of the near field profiles of the same silicon based light source. These are the cross-section near-field profiles of the horizontally oriented dipole (e) and the vertically oriented dipole (f) at 1550 nm. The radius and the height of the ITO pillar are 60 nm and 200 nm, respectively, and the distance from QD to the bottom of the pillar is 10 nm.



(a)



(b)



(c)

Fig. 8. Enhancement of the device efficiency, as the function of radius a and height h with (a) 1 QD, (b) 3 QDs and (c) 5 QDs, where the distance from QD to the bottom of the pillar is 10 nm and the dipoles are oriented vertically.

the same pillar. Moreover, their radiation properties will also determine the distribution of the polarizations and DOS, which will in turn influence the radiative efficiency of the QDs. Thus, simulations with several QDs can be more persuasive for the enhancement factor. With three QDs and five QDs, the profiles of enhancement share the similar pattern with that of a single QD, while the optimal enhancement increases to 28 and 30 folds, respectively, slightly higher than the former case, due to the additional interaction between dipoles. So far, all numerical calculations rely on FDTD. Since the geometric sizes are much shorter than the wavelength, it is inevitable that quasi-static field can be a better approximation, which enables us to use quasi-static method in our analytical deduction. However, seldom does commercial software adopt this algorithm, which will be considered in our further quasi-static numerical analysis.

5. Summary

We have demonstrated the physical processes and critical concepts of using nano-cavity located near QDs to enhance their quantum efficiency. Both the Purcell factor (characterizing the efficiency enhancement) and the radiative efficiency of the cavity have been considered in our theoretical model. The theoretical results for energy decay rate, effective mode volume and enhancement factor in these two cases (corresponding to the two kinds of polarizations of stimulating electric fields) have been developed. By using FDTD, we have considered two different orientations of dipoles, which can also be interpreted to some degree by the results of two kinds of stimulating polarizations, and based on this, we have obtained the criterion for the best sizes of pillars for enhancement. Merits of pillar include its easy formation in laboratory and more tunable variables. Low-collision-frequency (i.e., low-loss) ITO design and fabrication is the most critical factor aiming at better enhancement. In general, fabrication can guarantee that its value is as low as 10% of plasma frequency [30]. Moreover, it follows from our analysis (about the larger-size extent of localization for emission) that an inverted cone is absolutely a perfect structure, which can both confine the field and couple the SPP into photons efficiently. Furthermore, it is found that coupling between particles in a loose ordered array plays a negligible role. Though the interaction between particles has some negative effects, the problem can be solved by disordered arrangement. It is expected that revealing the physical essence and mechanism as well as design method for the present *plasmonic nano-particle-assisted light-emission enhancement* in quantum dots would be beneficial to many research fields, e.g., silicon based light sources and advanced solar cells [31].

Acknowledgments

This research was supported by the National Basic Research Program of China (973 Program, No. 2013CB632104), National Natural Science Foundation of China (Nos. 61575176 and 11174250), the Natural Science Foundation of Zhejiang Province of China (Nos. LZ12F04002 and LY16A040002), and the Research Foundation of State Key Laboratory of Modern Optical Instrumentation (MOI20150105).